Phonon anharmonicity of rutile SnO_{2} studied by Raman spectrometry and first principles calculations of the kinematics of phonon-phonon interactions

Tian Lan, Chen W. Li, and Brent Fultz

Phys. Rev. B **86**, 134302 — Published 11 October 2012

DOI: 10.1103/PhysRevB.86.134302

Phonon anharmonicity of rutile SnO_2 studied by Raman spectrometry and first principles calculations of the kinematics of phonon-phonon interactions

Tian Lan,* Chen W. Li, and Brent Fultz
Department of Applied Physics and Materials Science,
California Institute of Technology, Pasadena, California 91125, USA

Raman spectra of rutile tin dioxide (SnO_2) were measured at temperatures from 83 to 873 K. The pure anharmonicity from phonon-phonon interactions was found to be large and comparable to the quasiharmonicity. First principles calculations of phonon dispersions were used to assess the kinematics of 3-phonon and 4-phonon processes. These kinematics were used to generate Raman peak widths and shifts, which were fit to measured data to obtain the cubic and quartic components of the anharmonicity for each Raman mode. The B_{2g} mode had a large quartic component, consistent with the symmetry of its atom displacements. The broadening of the B_{2g} mode with temperature showed an unusual concave downwards curvature. This curvature is caused by a change with temperature in the number of down-conversion decay channels, originating with the wide band gap in the phonon dispersions.

I. INTRODUCTION

Rutile tin dioxide (SnO_2) is the most common and stable oxide of tin found in nature. Owing to the wide variety of its applications for optoelectronics, heterogeneous catalysis and gas sensors, rutile SnO_2 has been the subject of much recent research.[1] Lattice dynamics, phase transitions, and nanostructures of SnO_2 have been studied by measurements of optical phonons with Raman, Brillouin or infrared spectroscopy,[2–6] and by computation with force field models or density functional theory.[2,7–11] Rutile SnO_2 is tetragonal with the space group $P4/mnm$. The modes of symmetry B_{1g}, E_g, A_{1g} and B_{2g} are Raman active, and comprise motions of oxygen anions with respect to stationary tin cations, either perpendicular to the c axis (modes B_{1g}, A_{1g} and B_{2g}), or along the c axis (mode E_g).

Nonharmonic effects are known to be important for understanding the thermodynamic stability and the thermal transport properties of materials at elevated temperatures, but the anharmonic lattice dynamics of rutile SnO_2 is largely unknown. Perhaps the most complete experimental results are from Peercy and Morosin's work in 1973.[3] They reported frequency shifts of Raman modes with temperature and pressure, although the temperature range was below 480 K and no phonon broadening information was reported. The linewidth broadening of the A_{1g} mode was measured to 973 K by Sato and Asari, and compared well with results from shell model calculations.[8] Their results suggest that the anharmonicity of SnO_2 is large.

In our recent study on rutile TiO_2, the pure anharmonicity gave shifts of Raman peaks that were as large as from quasiharmonicity.[12] In that study we developed a rigorous method of simultaneously fitting Raman peak widths and shifts with calculations from the kinematics of phonon-phonon interactions. The effects of cubic and quartic anharmonicity were separated, and these anharmonic effects were found to be dominated by phonon kinematics. This previous work on TiO_2 used kinematics calculated with a shell model, but in the present study on rutile SnO_2, inconsistencies in the different shell model parameters from the literature motivated the use of *ab initio* methods to calculate phonon dispersions. The analysis and comparison of our present results on rutile SnO_2 with previous results on TiO_2 provides a better understanding of the anharmonic phonon dynamics in both.

Here we report high resolution measurements of Raman spectra at temperatures from 83 to 873 K. Both phonon frequency shifts and broadenings are reported. The quasiharmonic effects from thermal expansion were separated from the anharmonic effects of phonon-phonon interactions by comparing the temperature dependence to the pressure dependence of the Raman peaks. The data fitting method used *ab initio* calculations of two-phonon kinematic functionals to identify the effects of cubic and quartic anharmonicity. The peak broadening originates with cubic anharmonicity, but the peak shifts depend on both cubic and quartic effects. The phonon-phonon kinematics explains an unusual feature in the temperature dependence of the broadening of the B_{2g} mode of rutile SnO_2. The large difference in masses of Sn and O atoms causes a gap in the phonon density of states (DOS) that produces a peak in the two-phonon DOS (TDOS). The thermal shift moves the frequency of the B_{2g} mode away from this peak in the TDOS, and reduces the number of channels available for three-phonon processes, giving a concave-downwards curvature to the thermal broadening of the B_{2g} peak. The symmetrical B_{2g} mode was found to have a relatively large quartic anharmonicity.

II. EXPERIMENTAL PROCEDURES

Measurements were performed on both powder and single crystal samples of rutile SnO_2. The powder sample was prepared from commercial SnO_2 powder (Alfa Aesar, Ward Hill, MA) with a grain size of 10 μm. The powder was compressed into pellets of 1 mm thickness using a pressure of 50 MPa at ambient temperature. Raman spectra were acquired before and after compression into a pellet, and were found to be identical. A sample of single crystal casiterite of high optical quality was provided by the Mineral Museum of the Division of Geological and Planetary Sciences at the California Institute of Technology. The sample was cut and polished to a thickness of approximately 0.3 mm. Samples were mounted on the silver block of a Linkam thermal stage that provided excellent heat transfer and temperature stability for both heating and cooling. The sample chamber was sealed and purged with nitrogen gas flow. A temperature controller drove a 200 W power supply for heating. For low temperature measurements, the stage was equipped with a coolant pump that injected liquid nitrogen directly into the silver block. Samples of powder pellets were measured at temperatures from 83 to 833 K, and the single crystal sample was measured from 83 to 873 K. Each temperature was held stable for 10 min before the spectrum was taken. The temperature precision was within 1 K.

The Raman spectra were measured with a Renishaw micro-Raman system with an Olympus LMPlanFI microscope lens. The spectrometer was configured in backscattering geometry, minimizing issues with the thickness of the sample. A depolarized solid state laser operated at wavelength of 514.5 nm excited the sample with the low incident power of 10 mW to avoid additional thermal heating. The laser spot size was 12 μm in diameter. To test for heating effects this spot size was varied, but no changes were found. Each Raman spectrum was accumulated in 10

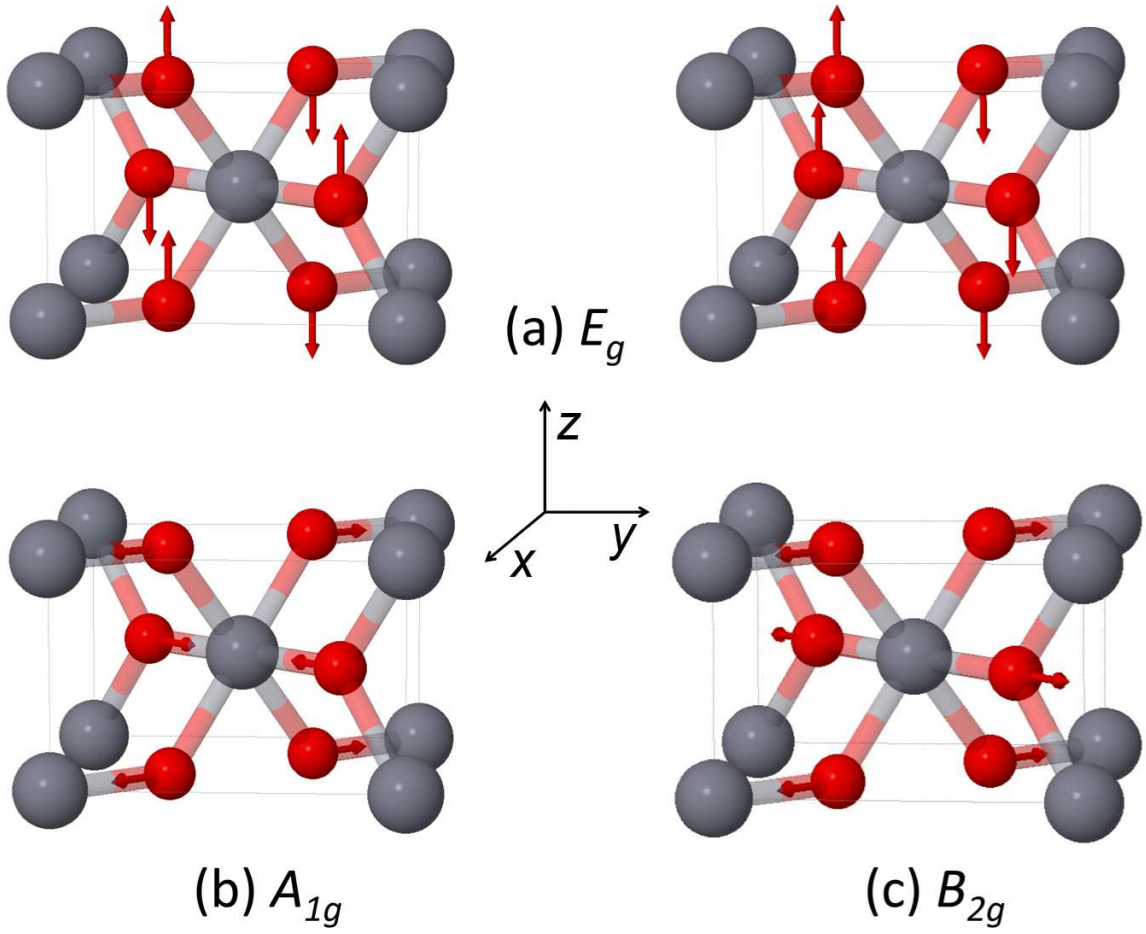

FIG. 1. Rutile structure and oxygen atom displacements for Raman-active modes.

measurements with 10 s exposure times.

III. RESULTS

Representative Raman spectra of powder samples are shown in Fig. 2. Three of the four Raman-active modes, E_g, A_{1g} and B_{2g}, have enough intensity for extracting quantitative information on phonon frequencies and linewidths. The B_{1g} mode was too weak for obtaining quantitative information (its intensity is about three orders of magnitude smaller than that of the A_{1g} mode[2]). The single crystal sample showed very similar spectra, but the E_g mode was weaker primarily because of orientation effects. Three weak abnormal Raman bands that were previously reported[13] were also observed at 503, 545 and 692 cm^{-1} for both powder and single crystal samples.

After background subtraction, each peak in each spectrum was fitted to a Lorentzian function to obtain a centroid and full-width-at-half-maximum (FWHM). The FWHM data from the experiment were corrected for the finite resolution of the spectrometer.[14] At room temperature, the Raman peak frequencies were 475 cm^{-1} for E_g, 633 cm^{-1} for A_{1g}, 774 cm^{-1} for B_{2g}. The mode frequencies at 83 K, ω(83 K), were 476 cm^{-1}, 636 cm^{-1} and 778 cm^{-1}. Figure 3 presents results of peak shifts and widths versus temperature. Here the peak shift $\Delta\omega$ is defined as $\omega(T) - \omega(83\,K)$. We find good agreement with the frequency shift data reported by Peercy and Morosin at temperatures below 480 K.[3] We also find good agreement with the linewidth broadening data of the A_{1g} mode reported by Sato and Asari to 900 K.[8]

With increasing temperature, the A_{1g} and B_{2g} modes undergo large shifts to lower frequencies and significant linewidth broadenings, but the E_g mode undergoes less shift and broadening. At high temperatures above 500 K, the broadening of the B_{2g} mode shows an unusual concave downward curvature, while the other two modes broaden linearly. At low temperatures, the B_{2g} mode has a much larger linewidth than the other two modes. The linewidth of

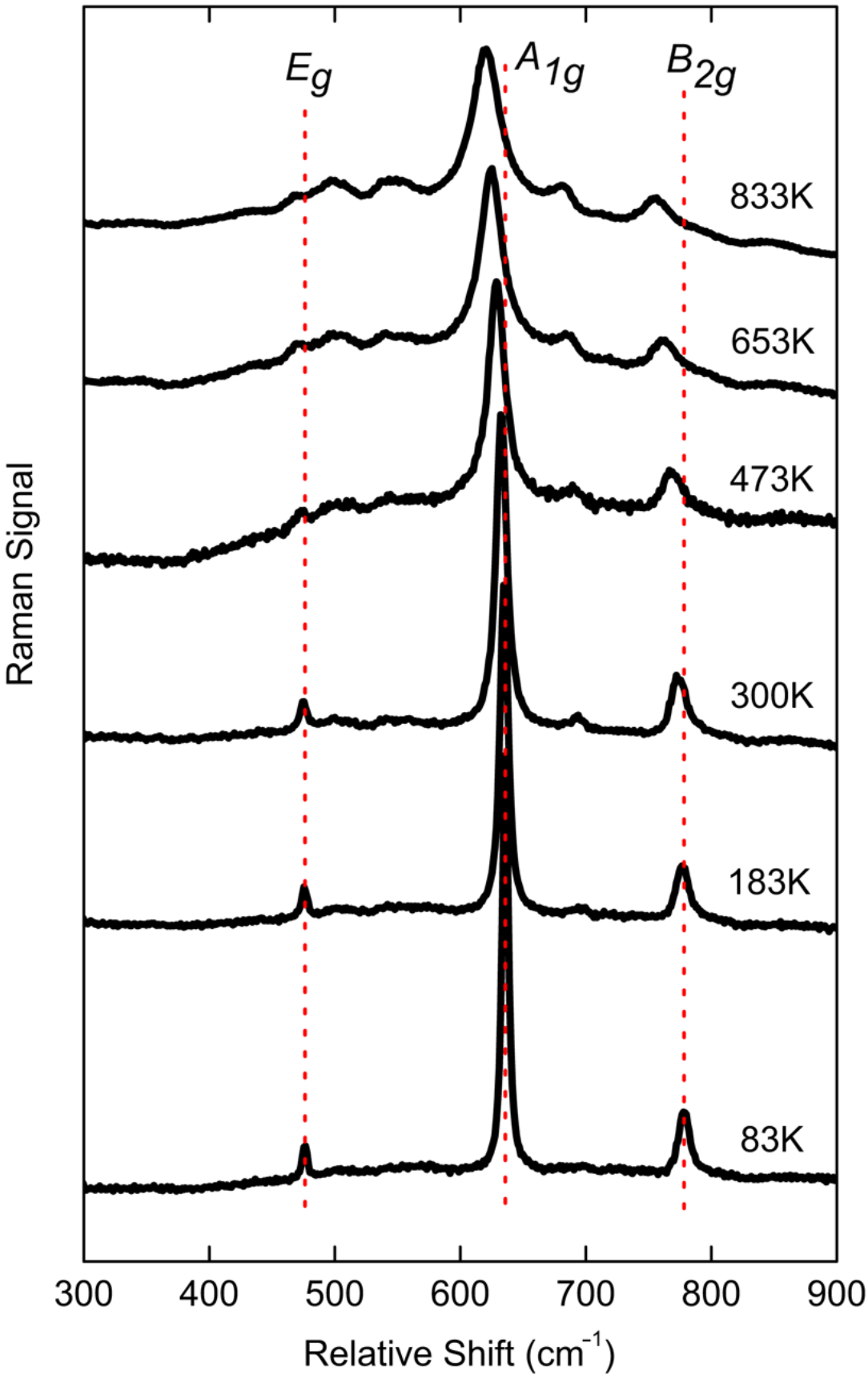

FIG. 2. Raman spectra of powder samples of rutile SnO_2 at selected temperatures.

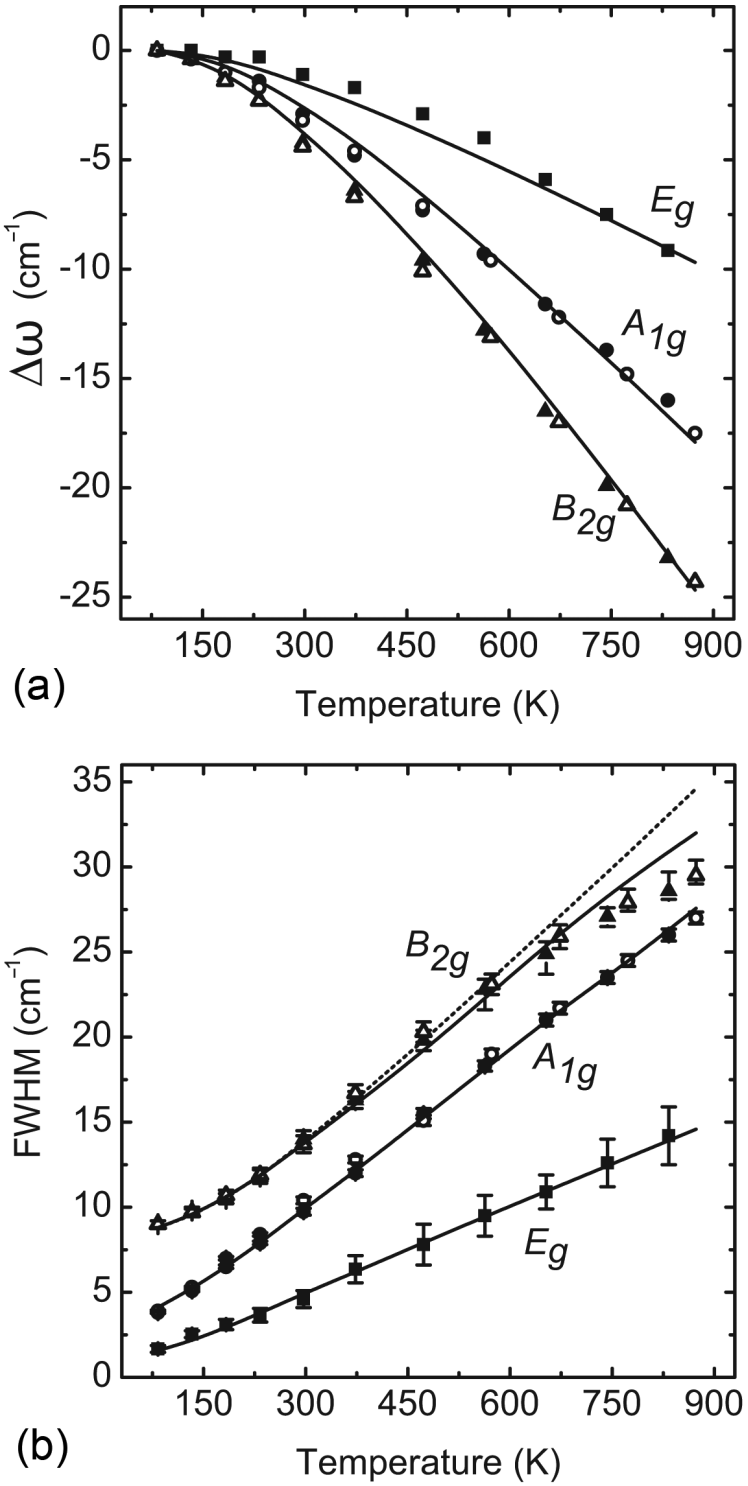

FIG. 3. Temperature dependence of (a) frequency shifts, (b) breadths as FWHMs, of the Raman modes E_g, A_{1g} and B_{2g}. The solid and open symbols represent the experimental data from powder and single crystal samples, respectively. Solid curves are the theoretical fittings with a full calculation of the kinematics of three- phonon and four-phonon processes. The dashed curve was calculated without considering the frequency dependence of $D_{0\downarrow}(\Omega)$, the number of decay channels, at elevated temperatures.

TABLE I. Comparison of the mode frequencies (cm^{-1}) at the Γ point for rutile SnO_2

Mode	Present Calc.	Calc.[a]	Calc.[b]	Expt.[c,d]
B_{1g}	104	83	100	121[d]
B_{1u}	147	138	140	-
$E_u^{(1)}(TO)$	223	200	236	244
$E_u^{(1)}(LO)$	269	252	268	276
$E_u^{(2)}(TO)$	285	270	297	293
$E_u^{(2)}(LO)$	335	307	377	366
A_{2g}	360	320	398	-
$A_{2u}(TO)$	456	457	512	477
E_g	468	462	476	476[d]
B_{1u}	564	553	505	-
$E_u^{(3)}(TO)$	613	584	651	618
A_{1g}	633	617	646	636[d]
$A_{2u}(LO)$	670	648	687	705
$E_u^{(3)}(LO)$	745	712	750	770
B_{2g}	765	734	752	778[d]

[a] First principles LDA calculation from Borges, *et al.*, Ref. [11]
[b] Force field calculation from Katiyar, *et al.*, Ref. [2]
[c] The data for infrared active modes at 100 K are from Katiyar, *et al.*, Ref. [2]
[d] The data for Raman-active modes at 83 K are from the present measurement.

the B_{2g} mode extrapolated to 0 K is approximately 8 cm^{-1}, whereas the linewidths of the E_g and A_{1g} modes extrapolate to less than 2 cm^{-1}.

IV. CALCULATIONS

A. First Principles Lattice Dynamics

Phonon dispersion calculations over the whole Brillouin zone were performed with the QuantumEspresso package, within the framework of *ab initio* density functional perturbation theory (DFPT).[15] Vanderbilt ultrasoft pseudopotentials with the local density approximation (LDA) and nonlinear core corrections were used. The LO/TO splitting was corrected by adding a non-analytical part into the dynamical matrix.[16] The calculated dispersion curves are shown in Fig. 4a, and mode frequencies at the Γ-point are presented in Table I. Calculations of the phonon density of states (DOS) with a uniform 16×16×16 sampling grid were also performed, as shown in Fig. 4b. Our calculations are in good agreement with prior experimental and theoretical results.[2,7–11] A band gap of width 100 cm^{-1}, centered around 400 cm^{-1}, is evident in Fig. 4. Above the gap, phonon modes are dominated by the motions of oxygen atoms.

B. The Kinematic Functionals $D^{\omega}(\Omega)$ and $P^{\omega}(\Omega)$

In anharmonic phonon perturbation theory,[17] the phonon linewidth is related to the two-phonon density of states (TDOS), $D(\Omega)$, which is defined as

$$\begin{aligned} D(\Omega) &= \sum_{\vec{q}_1, j_1} \sum_{\vec{q}_2 j_2} D(\Omega, \omega_1, \omega_2) \\ &= \frac{1}{N} \sum_{\vec{q}_1, j_1} \sum_{\vec{q}_2, j_2} \Delta(\vec{q}_1 + \vec{q}_2) \Big[(n_1 + n_2 + 1)\, \delta(\Omega - \omega_1 - \omega_2) \\ &\qquad + 2(n_1 - n_2)\, \delta(\Omega + \omega_1 - \omega_2) \Big] \end{aligned} \tag{1}$$

where Ω is the frequency of the initial phonon, and phonon modes $\{\vec{q}_i j_i\}$ have quasiharmonic frequencies $\{\omega_i\}$ and occupancies $\{n_i\}$. The first and second terms in square brackets are from down-conversion and up-conversion phonon

processes, respectively.[18]

The two-phonon kinematical functional $P(\Omega)$ for the anharmonic frequency shift is

$$P(\Omega) = \sum_{\vec{q}_1,j_1}\sum_{\vec{q}_2,j_2} P(\Omega,\omega_1,\omega_2)$$
$$= \frac{1}{N}\sum_{\vec{q}_1,j_1}\sum_{\vec{q}_2,j_2}\Delta(\vec{q}_1+\vec{q}_2)\,\wp\Big[\frac{n_1+n_2+1}{\Omega+\omega_1+\omega_2} - \frac{n_1+n_2+1}{\Omega-\omega_1-\omega_2}$$
$$+\frac{n_1-n_2}{\Omega-\omega_1+\omega_2} - \frac{n_1-n_2}{\Omega+\omega_1-\omega_2}\Big] \qquad (2)$$

where $\wp$ denotes the Cauchy principal part. The two-phonon spectra, $D(\Omega)$ and $P(\Omega)$, depend on temperature through the phonon occupancy factor, n. Both $D(\Omega)$ and $P(\Omega)$ were calculated at various temperatures from the first principles lattice dynamics calculations described in the previous subsection, sampling modes $\{\vec{q}j\}$ with a 16×16×16 q-point grid over the first Brillouin zone for good convergence.

V. ANALYSIS

A. Separating Anharmonicity from Quasiharmonicity

Both quasiharmonicity and pure anharmonicity contribute to the non-harmonic lattice dynamics of rutile SnO_2. In the quasiharmonic model, phonon modes behave harmonically with infinite lifetimes, but their frequencies are altered by the effects of volume on the interatomic potential. Pure anharmonicity originates with phonon-phonon interactions, which increase with temperature. Pure anharmonicity contributes to shifts in phonon frequencies, but also causes phonon damping and lifetime broadening of phonon peaks. The large peak broadenings in SnO_2 show that there are large effects from pure anharmonicity.

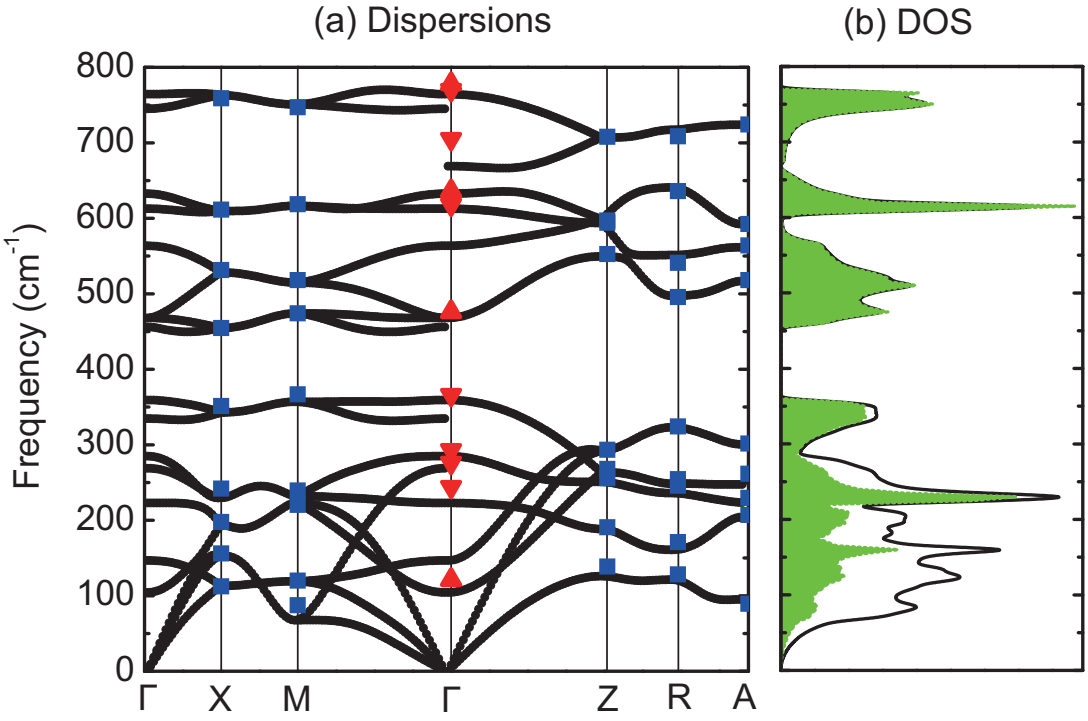

FIG. 4. (a) Calculated phonon dispersion along high symmetry directions of rutile SnO_2. $\Gamma\,(0,0,0)$, $X\,(0.5,0,0)$, $M\,(0.5,0.5,0)$, $Z\,(0,0,0.5)$, $R\,(0.5,0,0.5)$ and $A\,(0.5,0.5,0.5)$. At the Γ point, the frequencies from Table I are presented as up triangles (Raman) and down triangles (infrared). At the X, M, Z, R and A points, the mode frequencies from Ref. [9] (all doubly degenerate) are presented as squares. (b) Total phonon DOS (black curve) and oxygen-projected DOS (filled green).

TABLE II. Frequencies of the three Raman modes, mode Grüneisen parameters, and the logarithmic pressure and temperature derivatives of frequency.

Mode	$\omega(300\,K)$ (cm^{-1})	γ_j [a] [expt.]	γ_j [b] [calc.]	$\left(\frac{\partial \ln \omega}{\partial T}\right)_P$ ($10^{-5}K^{-1}$)	=	$-\gamma_j\beta$ [c] ($10^{-5}K^{-1}$)	+	$\left(\frac{\partial \ln \omega}{\partial T}\right)_V$ ($10^{-5}K^{-1}$)
E_g	475	1.45	1.48	-2.6		-1.7		-0.9
A_{1g}	633	1.65	1.81	-4.2		-1.9		-2.3
B_{2g}	774	1.49	1.71	-4.6		-1.7		-2.9

[a] Grüneisen parameters data from Hellwig, *et al.*, Ref. [4]
[b] From the present first principles calculations
[c] Thermal expansion data from Peercy and Morosin, Ref. [3]

To separate the peak shifts caused by pure anharmonicity from shifts caused by quasiharmonicity, we treat the mode frequency $\omega_j = \omega_j(V,T)$ as a function of volume and temperature[19]

$$\left(\frac{\partial \ln \omega_j}{\partial T}\right)_P = -\frac{\beta}{\kappa}\left(\frac{\partial \ln \omega_j}{\partial P}\right)_T + \left(\frac{\partial \ln \omega_j}{\partial T}\right)_V \tag{3}$$

where j is the phonon mode index, β is the volume thermal expansivity and κ is the isothermal compressibility. This is a general method to separate phonon quasiharmonicity from phonon anharmonicity, and is not unique for rutile structures, for example. The left-hand side gives the directly measurable temperature-dependent isobaric frequency shift, including both quasiharmonic and pure anharmonic behavior. The first term on the right-hand side, the isothermal frequency shift as a function of pressure, is the quasiharmonic contribution, which is also measureable. By defining a mode Grüneisen parameter as the proportionality of the relative change of the mode frequency to the relative change of volume, i.e., $\gamma_j = -\partial(\ln \omega_j)/(\partial(\ln V))$, the quasiharmonic term can be written as $\gamma_j\beta$. The second term on the right of Eq. 3 is the frequency shift from the pure anharmonicity, which depends on temperature and not volume. From the difference of the isobaric and isothermal frequency shifts, the pure anharmonicity can be determined experimentally.

To obtain the quasiharmonic contributions to the peak shifts, we used the mode Grüneisen parameters γ_j reported recently by Hellwig, *et al.*, from Raman measurements at pressures to 14 GPa,[4] which agreed well with earlier high pressure measurements to 4 GPa.[20] These results suggest that Peercy and Morosin overestimated the quasiharmonic contributions to their data, for which the pressure was only 0.4 GPa.

We also performed first principles calculations of the mode Grüneisen parameters by optimizing the enthalpy function to 10 GPa. Our calculated γ_j were in good agreement with the experimental results of Hellwig, *et al.*, and both are listed in Table II. Since the γ_j are very weakly dependent on temperature, as is the thermal expansion above 400 K,[3,19] the γ_j were assumed to be constants when assessing the volume dependent quasiharmonic contribution. The last two columns of Table II separate the measured isobaric temperature derivatives into the pure volume and pure temperature contributions as in Eq. 3. These last columns in Table II are the frequency shifts from quasiharmonicity and pure anharmonicity at temperatures above 400 K.

By comparing the last two columns in Table II, we see that like rutile TiO_2, the pure anharmonic contribution is comparable to the quasiharmonic contribution above 400 K. Nevertheless, the total anharmonicity of SnO_2 is considerably smaller than for TiO_2. For the modes A_{1g} and B_{2g} in SnO_2, the pure anharmonic contribution is larger than the quasiharmonic, while the E_g mode is more quasiharmonic. The relative magnitudes of pure anharmonicities of the three modes derived from the frequency shift data are consistent with the relative magnitudes of linewidth broadenings of the modes as shown in Fig. 3b.

B. Cubic and Quartic Anharmonicity

Anharmonicity tensors describe the coupling strengths for phonon-phonon interactions, but a prerequisite is that the phonons in these processes satisfy the kinematical conditions of conservation of energy and momentum. An anharmonicity tensor element for an s-phonon process is[21]

$$V(j;\vec{q}_1 j_1;...;\vec{q}_{s-1} j_{s-1}) = \frac{1}{2s!}\left(\frac{\hbar}{2N}\right)^{\frac{s}{2}} N\,\Delta(\vec{q}_1 + \cdots + \vec{q}_{s-1}) \times[\omega_{j0}\omega_1 \cdots \omega_{s-1}]^{\frac{1}{2}} C(j;\vec{q}_1 j_1;...;\vec{q}_{s-1} j_{s-1}) \tag{4}$$

where $\Delta(\vec{q}_1+\cdots+\vec{q}_{s-1})$ enforces momentum conservation and the $C(.)$'s, elements of the s-phonon anharmonic tensor, are expected to be slowly-varying functions of their arguments. The cubic anharmonicity tensor has been calculated by first principles methods,[18,22,23] but to our knowledge the the quartic anharmonicity tensor has never been fully calculated from first principles.

Nevertheless, if the anharmonicity tensor or its average does not vary significantly for different phonon processes, the coupling factor and the kinematic factor are approximately separable in Eq. 4. The separation of the anharmonic coupling and the kinematics has been used with success in many studies including our recent report on rutile TiO_2.[12] We consider the term $C(j;\vec{q}_1 j_1;...;\vec{q}_{s-1} j_{s-1})$ to be a constant of the Raman mode j, and use it as a fitting parameter. Although $C(j;\vec{q}_1 j_1;\vec{q}_2 j_2)$ and $C(j;j;\vec{q}_1 j_1;-\vec{q}_1 j_1)$ change with j_1 and j_2, an average over modes, $\langle C(.)\rangle = \sum_{1,2} C(j;\vec{q}_1 j_1;\vec{q}_2 j_2)/\sum_{1,2} 1$, is needed by the fitting, where 1, 2 under the summation symbol represent $\vec{q}_i j_i$. We define the cubic and quartic fitting parameters as

$$C_j^{(3)} = \langle C(j;\vec{q}_1 j_1;\vec{q}_2 j_2)\rangle \tag{5a}$$

$$C_j^{(4)} = \langle C(j;j;\vec{q}_1 j_1;-\vec{q}_1 j_1)\rangle \tag{5b}$$

To the leading order of cubic and quartic anharmonicity, the broadening of the Raman peaks is $2\Gamma^{(3)}(j;\Omega)$. The frequency shift of the Raman peaks is $\Delta^{Q}+\Delta^{(3)}+\Delta^{(3')}+\Delta^{(4)}$, where the quasiharmonic part Δ^{Q} is the integral form of the first term in Eq. 3. These quantities can be written as functions of $D(\Omega,\omega_1,\omega_2)$ and $P(\Omega,\omega_1,\omega_2)$, weighted by average anharmonic coupling strengths[12]

$$\begin{aligned}\Gamma^{(3)}(j;\Omega) &= \frac{\pi\hbar}{64}\omega_{j0}\left|C_j^{(3)}\right|^2 \sum_{\vec{q}_1,j_1}\sum_{\vec{q}_2,j_2}\omega_1\omega_2\, D(\Omega,\omega_1,\omega_2)\\ &= \omega_{j0}\left|C_j^{(3)}\right|^2 D^{\omega}(\Omega)\end{aligned} \tag{6a}$$

$$\begin{aligned}\Delta^{(3)}(j;\Omega) &= -\frac{\hbar}{64}\omega_{j0}\left|C_j^{(3)}\right|^2 \sum_{\vec{q}_1,j_1}\sum_{\vec{q}_2,j_2}\omega_1\omega_2\, P(\Omega,\omega_1,\omega_2)\\ &= \omega_{j0}\left|C_j^{(3)}\right|^2 P^{\omega}(\Omega)\end{aligned} \tag{6b}$$

$$\Delta^{(3')}(j) = -\frac{\hbar}{16N}\omega_{j0}\left|C_j^{(3)}\right|^2 \sum_{\vec{q}_2 j_2}\omega_{j_2}(\vec{q}_2)\left(n_{\vec{q}_2 j_2}+\tfrac{1}{2}\right) \tag{6c}$$

$$\Delta^{(4)}(j) = \frac{\hbar}{8N}\omega_{j0}C_j^{(4)} \sum_{\vec{q}_1 j_1}\omega_{j_1}(\vec{q}_1)\left(n_{\vec{q}_1 j_1}+\tfrac{1}{2}\right) \tag{6d}$$

where $D^{\omega}(\Omega)$ and $P^{\omega}(\Omega)$ are functionals of $D(\Omega,\omega_1,\omega_2)$ and $P(\Omega,\omega_1,\omega_2)$ weighted by the kinematics of anharmonic phonon coupling. Figure 5 shows representative results for $D^{\omega}(\Omega)$ and $P^{\omega}(\Omega)$ at 0 K and 800 K. The down-conversion and up-conversion subspectra are also shown.

The $\Delta^{(3')}$ is an additional low-order cubic term that corresponds to instantaneous three-phonon processes.[17] It is nonzero for crystals having atoms without inversion symmetry, as in the case for the oxygen atom motions in the A_{1g} mode. It is much smaller than other contributions, however, owing to symmetry restrictions.

With Eq. 6 and rigorous calculations of $D^{\omega}(\Omega)$ and $P^{\omega}(\Omega)$ at various temperatures, for each Raman mode both its frequency shift and broadening were fitted simultaneously with the two parameters, $|C_j^{(3)}|^2$ and $C_j^{(4)}$. The best fits for the shifts and broadenings are shown in Fig. 3, and the fitting parameters are given in Table III. Figure 6 also shows contributions to the shift from the quasiharmonic and pure anharmonicity (dashed curves).

With a single parameter $|C^{(3)}|^2$ for each mode, good fittings to the broadenings are obtained as shown in Fig. 3b, indicating significant cubic anharmonicity for these Raman-active modes. Moreover, our fittings also successfully reproduced the unusual concave curvature of the B_{2g} mode at high temperatures. The $|C_j^{(3)}|^2$ do not vary much among different modes, suggesting the assumption of slowly-varying properties of $C(.)$'s is reasonable.

TABLE III. Fitting parameters for the temperature dependent Raman modes (unit: 10^{10} erg^{-1})

	E_g	A_{1g}	B_{2g}
$\lvert C^{(3)}\rvert^2$	0.87	1.6	1.0
$-C^{(4)}$	1.0	2.6	7.3

Starting with the same cubic fitting parameters used for the broadenings, the frequency shifts of these modes are fit well by adding the quasiharmonic and quartic anharmonic effects. As shown in Fig. 6, the quartic contribution $\Delta^{(4)}$ is generally of the same order as the cubic contribution $\Delta^{(3)}$, consistent with the fact that $\Delta^{(4)}$ and $\Delta^{(3)}$ are both leading-order terms for the anharmonic frequency shifts. For the E_g and A_{1g} modes, the pure anharmonicity is mainly from the cubic terms, but for the B_{2g} mode, the quartic anharmonicity is dominant and is as large as the quasiharmonic part.

VI. DISCUSSION

We can understand why the B_{2g} mode has a relatively larger quartic anharmonicity than the A_{1g} from differences in how the O atoms move towards the Sn atoms. Using a unit cell with 4 O atoms and 2 Sn atoms, as shown in Fig. 1, the A_{1g} mode has all 4 O atoms moving directly into one Sn atom on one half of the cycle, but moving between two Sn atoms during the other half cycle. The B_{2g} mode has 2 O atoms moving into a Sn atom and 2 O atoms moving between two Sn atoms on both halves of the vibrational cycle, making for a potential that is an even function of the

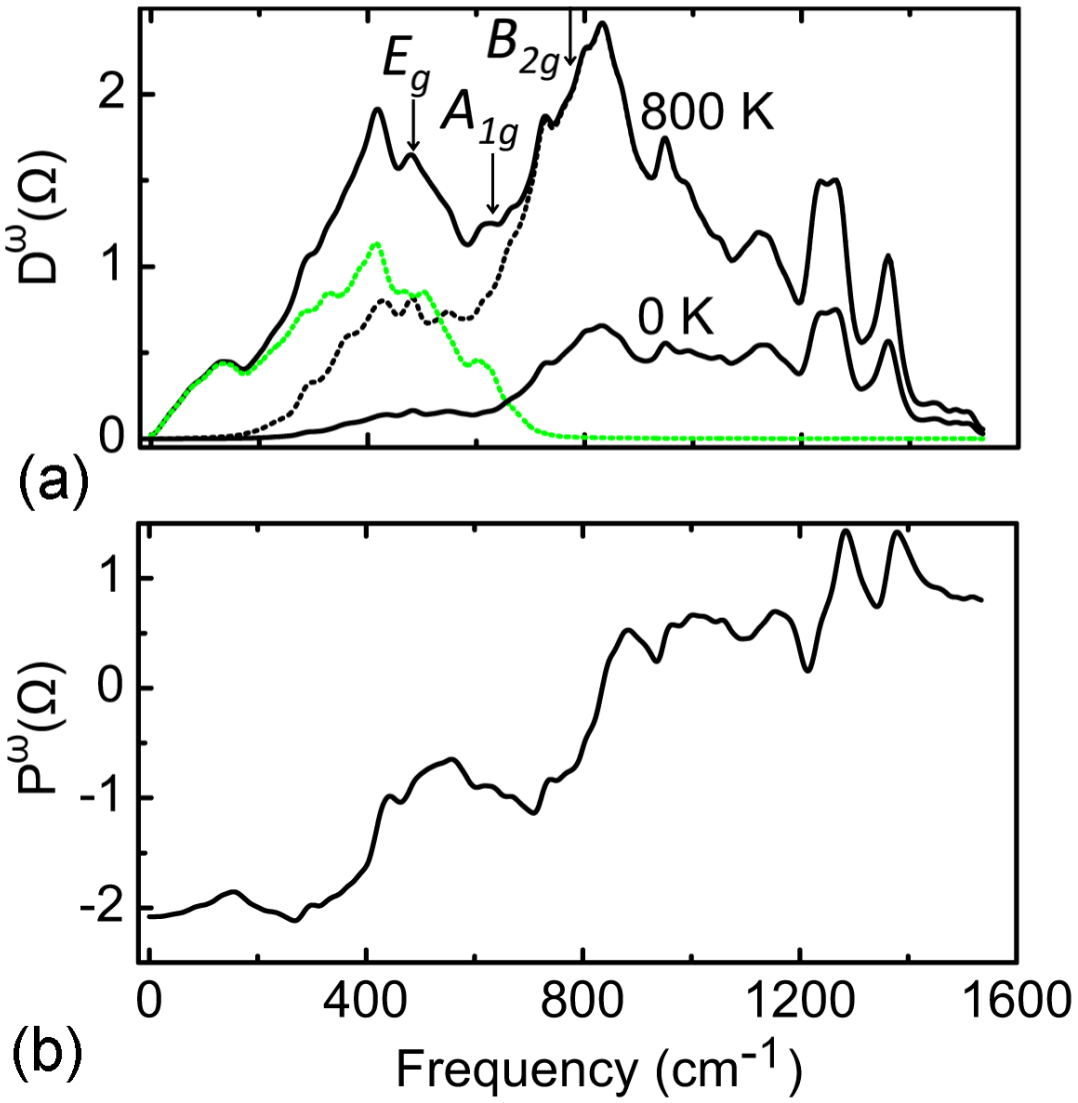

FIG. 5. (a) Two-phonon density of states $D^{\omega}(\Omega)$ for 0 K and 800 K. The arrowheads mark the positions of the three Raman modes, E_g, A_{1g} and B_{2g}, respectively. The up-conversion and down-conversion contributions at 800 K are shown in green and black dash curves, respectively. There is no up-conversion process at 0 K. (b) $P^{\omega}(\Omega)$ at 800 K.

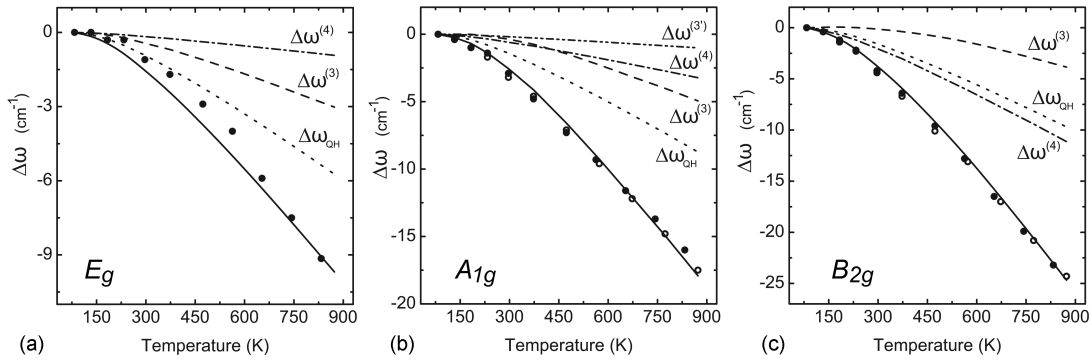

FIG. 6. Fittings of the temperature dependence of frequency shift of (a) the E_g mode, (b) the A_{1g} mode and (c) the B_{2g} mode. Solid curves are the final fittings to $\Delta^{Q} + \Delta^{(3)} + \Delta^{(3')} + \Delta^{(4)}$. Different contributions are indicated individually in these figures.

phonon coordinate. Table III shows a larger quartic contribution for the B_{2g} mode than the A_{1g}. (The E_g mode does not have similar atom motions for comparison.)

The TDOS function $D^{\omega}(\Omega)$ in Fig. 5 shows large variations with Ω that explains a trend in the thermal broadening of Fig. 3b. Owing to the high frequency of the B_{2g} mode, at the temperatures of this study its phonon-phonon anharmonicity comes mostly from down-conversion processes, as shown in Fig. 5. Ignoring the small up-conversion contribution, at high temperatures[24]

$$D^{\omega}(\Omega, T) \propto T \sum_{\vec{q}_1, j_1} \sum_{\vec{q}_2, j_2} \delta(\Omega - \omega_1 - \omega_2) \equiv T\, D_{0\downarrow}(\Omega) \tag{7}$$

where $D_{0\downarrow}(\Omega)$ is the number of two-phonon down-conversion channels. Usually the line broadening is linear in T because $D_{0\downarrow}(\Omega)$ does not vary much with temperature. However, the B_{2g} mode at 774 cm^{-1} lies on a steep gradient of $D^{\omega}(\Omega, T)$ in Fig. 5. Because the B_{2g} mode undergoes a significant shift of frequency with temperature, it moves down the gradient of $D^{\omega}(\Omega, T)$, and its broadening is less than linear in T. The temperature dependence of the broadening of the B_{2g} mode has an unusual concave downwards shape. For comparison, the dashed line in Fig. 3 was calculated without considering the frequency dependence of $D_{0\downarrow}(\Omega)$ at elevated temperatures, and it deviates substantially from the experimental trend.

The unusual temperature dependence of the linewidth of the B_{2g} mode comes from the sharp peak in $D^{\omega}(\Omega, T)$ centered at 800 cm^{-1}. This feature in the TDOS originates with the phonon DOS of SnO_2 shown in Fig. 4, which has a band gap between 360 cm^{-1} to 450 cm^{-1} associated with the mass difference of Sn and O atoms. The shape of the TDOS can be understood as the convolution of the phonon DOS with itself. With two approximately equal regions above and below the gap, the result is a peak at 800 cm^{-1}, with steep slopes on both sides. For comparison, although the TDOS of rutile TiO_2 is shaped as a broad peak,[12] it does not have the sharp features of Fig. 5a because the mass difference between Ti and O atoms does not cause a band gap in the phonon DOS of TiO_2.

Especially with more up-conversion processes at higher temperatures, there is another peak in the SnO_2 TDOS at 400 cm^{-1}. The up-conversion channels are primarily from the pairs of sharp peaks in the phonon DOS at 100 cm^{-1} and 500 cm^{-1}, 200 cm^{-1} and 600 cm^{-1}, and 350 cm^{-1} and 750 cm^{-1}. Although the E_g mode at 475 cm^{-1} is on the slope of this peak in the TDOS, the E_g mode does not show anomalous broadening with temperature because it undergoes only a small thermal shift in frequency.

In the low-temperature limit, up-conversion processes are prohibited because $n \to 0$. The peak linewidth extrapolated to 0 K is determined entirely by down-conversion processes, quantified by the down-conversion TDOS.[24] The B_{2g} mode has a significant broadening because its frequency is near a peak in the down-conversion TDOS, as seen in Fig. 5. On the other hand, the E_g and A_{1g} modes are not broadened at low temperatures because their frequencies are at low values of the TDOS. The phonon-phonon kinematics accounts for the significant difference of linewidths between the B_{2g} and the other two Raman modes at low temperatures.

VII. CONCLUSIONS

Raman spectra were measured on rutile SnO_2 at temperatures from 83 to 873 K, and large anharmonic shifts and broadenings were found for the three measurable Raman peaks. Individual assessments of the cubic and quartic

contributions to the anharmonicity were performed by calculating the kinematics of 3-phonon and 4-phonon processes with *ab initio* methods, and varying the anharmonic coupling parameters to fit the peak shifts and broadenings simultaneously. The quartic anharmonicity of the B_{2g} mode was found to be large, unlike the E_g and A_{1g} modes for which cubic anharmonicity is dominant. The quartic behavior of the B_{2g} mode can be understood from the symmetry of the oxygen atom displacements.

The phonon DOS of SnO_2 has a band gap around $400\,\mathrm{cm}^{-1}$ owing to the mass difference of Sn and O atoms, with similar structure above and below the gap. This causes a sharp peak in the TDOS at $800\,\mathrm{cm}^{-1}$. The frequency of the B_{2g} mode is on the slope of this peak in the TDOS, and its frequency shift with temperature reduces the number of down-conversion channels for its broadening. The thermal broadening of the B_{2g} mode consequently shows an anomalous concave downwards curvature. At 0 K, the large TDOS around $800\,\mathrm{cm}^{-1}$ explains the large linewidth of the B_{2g} mode. The anharmonic peak shifts and broadenings were well accounted for by the kinematics of phonon-phonon interactions, suggesting that on the average, the anharmonicity tensors for rutile SnO_2 are not rich in structure.

ACKNOWLEDGMENTS

We thank George R. Rossman for help with the micro-Raman work and sample preparation. This work was supported by DOE BES under contract DE-FG02-03ER46055. The work benefited from software developed in the DANSE project under NSF award DMR-0520547.

* tianlan@caltech.edu

[1] M. Batzill and U. Diebold, Prog. Surf. Sci. **79**, 47 (2005).
[2] R. S. Katiyar, P. Dawson, M. M. Hargreave, and G. R. Wilkinson, J. Phys. C: Solid St. Phys. **4**, 2421 (1971).
[3] P. S. Peercy and B. Morosin, Phys. Rev. B **7**, 2779 (1973).
[4] H. Hellwig, A. F. Goncharov, E. Gregoryanz, H.-K. Mao, and R. J. Hemley, Phys. Rev. B **67**, 174110 (2003).
[5] T. Livneh, Y. Lilach, I. Popov, A. Kolmakov, and M. Moskovits, J. Phys. Chem. C **115**, 17270 (2011).
[6] A. Diéguez, A. Romano-Rodríguez, A. Vilà, and J. R. Morante, J. Appl. Phys. **90**, 1550 (2001).
[7] F. Gervais and W. Kress, Phys. Rev. B **31**, 4809 (1985).
[8] T. Sato and T. Asari, J. Phys. Soc. Japan **64**, 1193 (1995).
[9] K. Parlinski and Y. Kawazoe, Eur. Phys. J. B **13**, 679 (2000).
[10] H. W. Leite Alves, C. C. Silva, A. T. Lino, P. D. Borges, L. M. R. Scolfaro, and E. F. da Silva, Jr., Appl. Surf. Sci. **255**, 752 (2008).
[11] P. D. Borges, L. M. R. Scolfaro, H. W. Leite Alves, and E. F. da Silva, Jr., Theor. Chem. Acc. **126**, 39 (2010).
[12] T. Lan, X. Tang, and B. Fultz, Phys. Rev. B **85**, 094305 (2012).
[13] F. Wang, X. Zhou, J. Zhou, T.-K. Sham, and Z. Ding, J. Phys. Chem. C **111**, 18839 (2007).
[14] J. Menéndez and M. Cardona, Phys. Rev. B **29**, 2051 (1984).
[15] P. Giannozzi, S. Baroni, N. Bonini, M. Calandra, R. Car, C. Cavazzoni, D. Ceresoli, G. L. Chiarotti, M. Cococcioni, I. Dabo, A. Dal Corso, S. de Gironcoli, S. Fabris, G. Fratesi, R. Gebauer, U. Gerstmann, C. Gougoussis, A. Kokalj, M. Lazzeri, L. Martin-Samos, N. Marzari, F. Mauri, R. Mazzarello, S. Paolini, A. Pasquarello, L. Paulatto, C. Sbraccia, S. Scandolo, G. Sclauzero, A. P. Seitsonen, A. Smogunov, P. Umari, and R. M. Wentzcovitch, J. Phys.: Condens. Matter. **21**, 395502 (2009).
[16] S. Baroni, S. de Gironcoli, A. Dal Corso, and P. Giannozzi, Rev. Mod. Phys. **73**, 515 (2001).
[17] A. A. Maradudin and A. E. Fein, Phys. Rev. **128**, 2589 (1962).
[18] X. Tang, C. W. Li, and B. Fultz, Phys. Rev. B **82**, 184301 (2010).
[19] G. A. Samara and P. S. Peercy, Phys. Rev. B **7**, 1131 (1973).
[20] J. F. Mammone, M. Nicol, and S. K. Sharma, J. Phys. Chem. Solids **42**, 379 (1981).
[21] I. P. Ipatova, A. A. Maradudin, and R. F. Wallis, Phys. Rev. **155**, 882 (1967).
[22] A. Debernardi, Phys. Rev. B **57**, 12847 (1998).
[23] G. Deinzer, G. Birner, and D. Strauch, Phys. Rev. B **67**, 144304 (2003).
[24] X. Tang and B. Fultz, Phys. Rev. B **84**, 054303 (2011).